Experimental Evidence of Accelerated Seismic Release without Critical Failure in Acoustic Emissions of Compressed Nanoporous Materials

Jordi Baró,[1,2,3,*] Karin A. Dahmen,[1] Jörn Davidsen,[2] Antoni Planes,[3] Pedro O. Castillo,[3,4] Guillaume F. Nataf,[3,5] Ekhard K. H. Salje,[6] and Eduard Vives[3,†]

[1]*Department of Physics, University of Illinois at Urbana Champaign, Urbana, Illinois 61801, USA*
[2]*Department of Physics and Astronomy, University of Calgary, 2500 University Drive NW Calgary, Alberta T2N 1N4, Canada*
[3]*Departament de Física de la Matèria Condensada, Facultat de Física, Universitat de Barcelona, Martí i Franquès, 1. 08028 Barcelona, Catalonia, Spain*
[4]*CONACYT, Instituto Tecnológico de Oaxaca, Av. Ing. Víctor Bravo Ahuja 125, Oaxaca de Juárez 68030, México*
[5]*Department of Materials Science, University of Cambridge, 27 Charles Babbage Road, Cambridge CB3 0FS, United Kingdom*
[6]*Department of Earth Sciences, University of Cambridge, Downing Street, Cambridge CB2 3EQ, United Kingdom*

(Received 25 March 2018; published 12 June 2018)

The total energy of acoustic emission (AE) events in externally stressed materials diverges when approaching macroscopic failure. Numerical and conceptual models explain this accelerated seismic release (ASR) as the approach to a critical point that coincides with ultimate failure. Here, we report ASR during soft uniaxial compression of three silica-based (SiO_2) nanoporous materials. Instead of a singular critical point, the distribution of AE energies is stationary, and variations in the activity rate are sufficient to explain the presence of multiple periods of ASR leading to distinct brittle failure events. We propose that critical failure is suppressed in the AE statistics by mechanisms of transient hardening. Some of the critical exponents estimated from the experiments are compatible with mean field models, while others are still open to interpretation in terms of the solution of frictional and fracture avalanche models.

DOI: 10.1103/PhysRevLett.120.245501

The mechanical deformation and failure of materials is a well-documented case of avalanche dynamics [1–33]. The energy of mechanical avalanches is partially released in elastic waves that can be detected by means of acoustic emission (AE) measurement [34]. Several studies suggested the presence of a phase transition associated with the ultimate failure point [18–22,35] which could, in theory, be monitored and forecast by means of the statistical analysis of the preceding AE activity [6,36–38] and be used for hazard assessment. AE signals recorded during mechanical tests usually display a scale-free distribution of energies (E) close to a power law: $D(E)dE \sim E^{-\varepsilon}dE$ with exponent $1 \lesssim \varepsilon \lesssim 2.5$. Three different relationships are often reported between this scale-free phenomenon and the proximity to failure: (i) The exponent ε in AE can decrease before failure [39–44]. (ii) The rate of energy released over time in AE experiments [45–49] diverges as a power law with an exponent m with respect to the time of failure t_c:

$$dE/dt(t) \propto (t_c - t)^{-m}, \qquad (1)$$

a phenomenon called accelerated seismic release (ASR) [50]. (iii) The characteristic scales of the avalanches depend on the distance to failure [25–28]. This latter observation supports the well-established idea that failure occurs due to the divergence of correlation lengths at a critical point [15,20,57,58]. This so-called critical failure hypothesis predicts a generalized homogeneous distribution of event energies:

$$D(E;f)dE = E^{-\varepsilon}\mathcal{D}(Ef^{\beta})dE = f^{\beta\varepsilon}\tilde{\mathcal{D}}(Ef^{\beta})dE, \qquad (2)$$

where $\mathcal{D}(x)$ and $\tilde{\mathcal{D}}(x)$ are scaling functions, $f \equiv 1 - t/t_c$ is the time to failure, and β is a characteristic exponent of the model.

While the exponent decrease (i) is currently not understood from a model perspective, ASR (ii) and critical failure (iii) are well reproduced by most micromechanical models [15–17,37,57]. Since all statistical n-moments diverge at failure as $\langle E^n \rangle \sim f^{(\varepsilon-1-n)\beta}$ and the activity rate (dN/dt) is constant in most micromechanical models, ASR (ii) is a natural outcome of critical failure:

$$dE/dt(f) = \langle E \rangle (f) dN/dt(f) \sim f^{(\varepsilon-2)\beta}. \qquad (3)$$

Although ASR is assumed as a signature of criticality [52,57], its connection with Eq. (2) is rarely tested with AE. Here, we analyze the AE during the approach to failure of nanoporous materials under soft uniaxial compression. We prove that ASR (ii) can appear in the absence of progressive exponent changes (i) or critical failure (iii). We estimate the experimental exponents m [Eq. (1)], ε [Eq. (2)], and γ,

TABLE I. Sample details: cross-sectional area A, height h, compression rate dP/dt, number N of recorded signals above threshold Th.

	Area A (mm^2)	Height h (mm)	Driving rate dP/dt (kPa/s)	Th (dB)	N
Vycor (V32)	17.0	5.65	5.7	23	34 138
Gelsil (G26)	46.7	6.2	0.7	26	5 412
Sands. (SR2)	17.0	4.3	2.4	23	27 271

relating the characteristic E of an event with its duration T through the conditional average:

$$\langle E|T\rangle \propto T^{\gamma}, \tag{4}$$

and interpret them in terms of the mean field solutions of fracture and frictional avalanches.

We limit our analysis to the three silica (SiO_2)–based materials studied in Ref. [5]: natural red sandstone (SR2, $\Phi = 17\%$ porosity) extracted from Arran Isle (United Kingdom) and two artificial porous silica glasses, Gelsil (Gel26, $\Phi = 36\%$) and Vycor (V32, $\Phi = 40\%$). Experimental details are found in Ref. [5] and summarized in Table I. Samples are compressed without lateral confinement at a steady quasistatically slow loading rate $dP/dt \sim 1$ kPa/s, equivalent to a strain rate $(d\epsilon/dt) \sim 10^{-5}\ \mathrm{s}^{-1}$ during quasielastic deformation. The sample height (h) is measured over time with a laser extensometer, and the AE is recorded by a piezoelectric transducer attached to the upper compression plate. Individual AE events are identified by thresholding the acoustic signal $V(t)$, defining the hitting time t_{AE} and duration D_{AE} of each AE event. The AE energy of each event is computed as $E_{\mathrm{AE}} \propto \int_{t_{\mathrm{AE}}}^{t_{\mathrm{AE}}+D_{\mathrm{AE}}} |V(t)|^2 dt$.

Figure 1 shows the relations between AE energy (E_{AE}) and duration (D_{AE}) in a density map, and the conditional averages $\langle D_{\mathrm{AE}}\rangle(E_{\mathrm{AE}})$. The experimental data are compared to a nonstochastic model considering a scale-free avalanche profile [Eq. (4)] and the best value of γ found by inspection (see Supplemental Material [59]). Within error bars (± 0.4), all values are compatible with $\gamma = 3$, as predicted by mean field (MF) models [60,61]. The density clouds fill narrow stripes around the conditional average values as expected by Eq. (4).

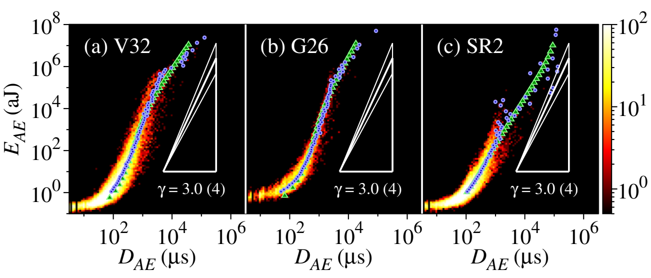

FIG. 1. Histograms (color-coded) of AE events in the duration-energy (D_{AE}, E_{AE}) space. Blue dots: Conditional averages $\langle D_{\mathrm{AE}}\rangle(E_{\mathrm{AE}})$. Green triangles: Numerical solutions of $E_{\mathrm{AE}}(D_{\mathrm{AE}})$ consistent with Eq. (4) (see main text for details), with $\gamma = 3.0(4)$ for V32, $\gamma = 3.4(4)$ for G26, and $\gamma = 3.2(4)$ for SR2.

The activity rate—the number of AE events per time unit—is nonstationary, as is also reported in Refs. [4–9]. Figure 2(a) shows the mechanical evolution expressed as a decrease in sample height $[h(t)]$ and the cumulative number of AE events $[N(t)]$ for the experiment V32. Figure 2(b) shows the activity rate (dN/dt) and the decrease in height (dh/dt) evaluated in intervals of uniaxial pressure $\Delta P = 100$ kPa (converted from t by dP/dt in Table I). We identify several sharp drops in h (five in Fig. 2), with a short characteristic temporal span $\Delta t_c \approx 0.1$ s (or $\Delta P \approx 100$ Pa), at pressure values P_c^k. These so-called strain drops are outliers to an otherwise smooth strain evolution, as observed in the dh/dP profile, and match a simultaneous increase of AE activity (dN/dP) and strong AE events. The events at P_c^k resemble brittle failure, a typical outcome of internal weakening or progressive damage in MF micromechanical models [10,62]. Brittle failure events are macroscopic by definition. Thus, during a loading cycle, a single (not multiple) brittle event is expected in these models. Here, however, the material recovers the stiffness during the intervals $P_c^k < P < P_c^{k+1}$ (Fig. 2). This can be explained by hardening, as reported in compression experiments [12], due to the accommodation of the stress field. The presence of both weakening and hardening localizes damage in brittle events that can correspond to spallation, correcting boundary defects [63] or be arrested due to stress heterogeneities [64]. An ultimate

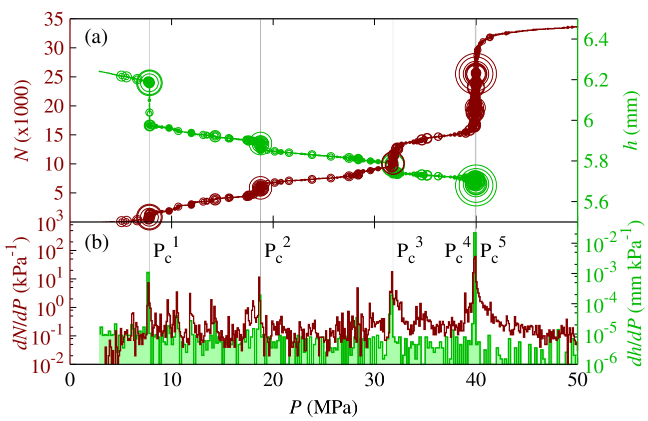

FIG. 2. Mechanical response and AE sequence for experiment on Vycor (V32). (a) Cumulative number of events N (dark red) and height evolution h (light green) in experiment V32 as a function of uniaxial pressure P. The size of the circles depends on the AE energy (size $\sim E_{\mathrm{AE}}^{0.25}$). (b) Mean AE activity rate dN/dt (dark red histograms) and strain rate dh/dt (light green histograms) in intervals of $\Delta P = 100$ kPa. Vertical gray lines: P_c^k.

system-sized failure event collapsing the whole sample is observed in all experiments (P_c^5 in Fig. 2 has an associated $\Delta h \sim 5$ mm).

We study how the statistics of AE events are modified close to the most prominent stress drops by evaluating $\langle E_{\mathrm{AE}}\rangle$, ε and dE_{AE}/dt in short stress intervals correlated with the distance to each strain drop: $f_k \coloneqq 1 - P/P_c^k$. We select P_c^k as the onset of each strain drop, identified with a precision of 0.01 s (equivalent to $\delta f_k \sim 10^{-6} - 10^{-5}$) and compare the results to Eq. (2) where $\mathcal{D}$ is an exponential cutoff:

$$D(E; E_m, E_c, \varepsilon) dE = E^{-\varepsilon} \frac{E_c^{\varepsilon - 1} \exp(-\frac{E}{E_c})}{\Gamma(1-\varepsilon, \frac{E_m}{E_c})} dE. \quad (5)$$

Here, $\Gamma(a, x)$ is the incomplete gamma function and E_m is the lower boundary of the distribution. E_c is the characteristic scale of the exponential cutoff and, according to critical failure, should be proportional to $f_k^{-\beta}$ [Eq. (2)]. We truncate the distribution at the lower boundary $E_m = 1$ aJ to avoid resolution artifacts distorting the power law for low energies.

We inquire if the strain drops at P_c^k can be interpreted as independent failure events, identified by at least one of the three trademarks mentioned earlier. Figures 3(a)–3(c) show the exponents $\hat{\varepsilon}(f_k)$ estimated by maximum likelihood inside the interval 1–1000 aJ [65] (overhat denotes estimation), compared to the global estimated exponent (gray line). Figures 3(d)–3(f) show the mean energy of individual AE events ($\langle E_{\mathrm{AE}}\rangle(f_k)$ in dots) compared to the solution to Eq. (5) (triangles) with $\hat{\varepsilon}(f_k)$ from Figs. 3(a)–3(c) and stationary $\hat{E}_c$ (gray lines). The lower panels [Figs. 3(g)–3(i)] show the rate of energy released by all events in temporal intervals ($dE_{\mathrm{AE}}/dP(f_k)$ in dots). In Figs. 3(g)–3(i), since some avalanches last longer than the evaluation intervals close to failure, their AE energy is split into intervals of 1 ms in order to increase the temporal resolution. The exponent $\hat{\varepsilon}(f_k)$ is almost stationary except for a few low values in the last intervals before P_c^k. Since all $\hat{\varepsilon}(f_k) < 2$, critical failure expects a divergence in $\langle E_{\mathrm{AE}}\rangle$ when $f_k \to 0$. As first reported in Vycor [4], $\langle E_{\mathrm{AE}}\rangle(f_k)$ is instead almost stationary and compatible with a finite and constant $\hat{E}_c$ (see E_{AE} distributions in the Supplemental Material [59]). Only the last intervals prior to failure show higher $\langle E_{\mathrm{AE}}\rangle(f_k)$, close to the 90% confidence interval limit. Despite the stationary $\langle E_{\mathrm{AE}}\rangle$, all data sets exhibit a steady increase in dE_{AE}/dt starting far from failure [Figs. 3(g)–(i)], as predicted by ASR [Eq. (1)] considering $m \sim 1.0$ (thin gray lines). Thus, we observe ASR, even when avalanches are noncritical.

Figure 3 illustrates how ASR [Eq. (1)] is more general than critical failure [Eq. (2)]. This result can be reproduced

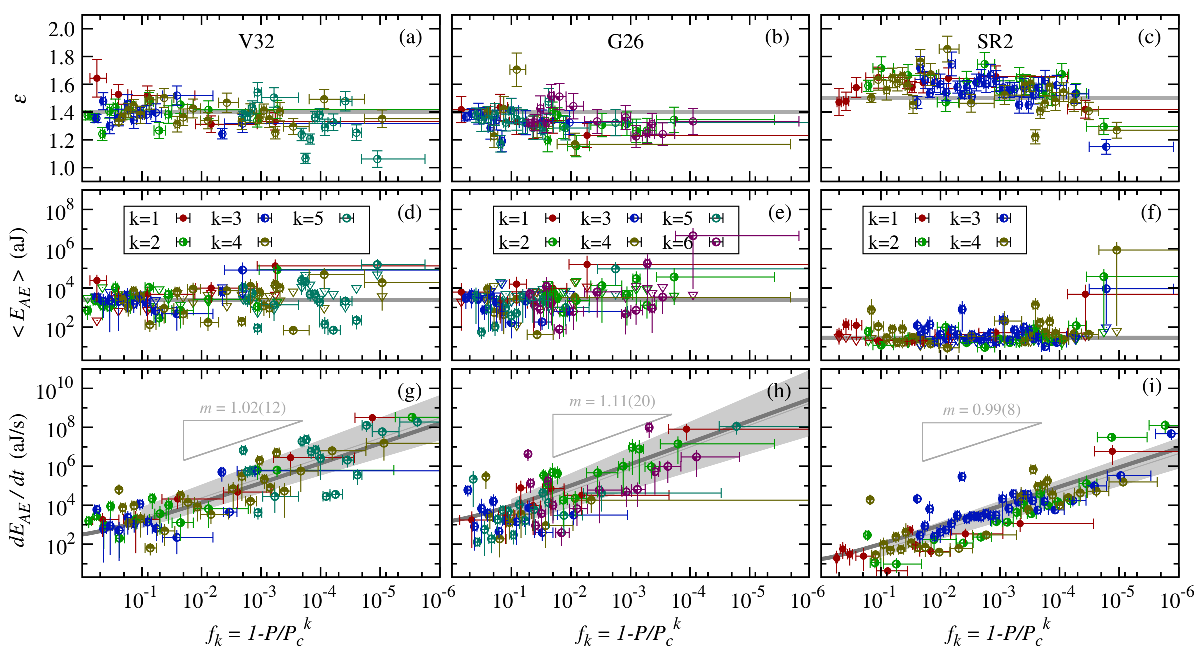

FIG. 3. Statistical variations with distance to strain drops P_c^k. The color scheme identifies the index k. (a)–(c) Exponent $\hat{\varepsilon}(f_k)$ from Eq. (2) estimated within the interval (1.0–1000 aJ). (d)–(f) Mean energy per signal $\langle E_{\mathrm{AE}}\rangle(f_k)$; expected mean value according to $D(E; E_m, E_c, \hat{\varepsilon}(f_k))$ (triangles) with $E_c = 10^6$ aJ (10^4 aJ for SR2); expected value from the global exponent (gray line). (g)–(i) Rate of AE energy dE_{AE}/dt. Thin gray line: Exponent m fitted by least squares within $10^{-6} < f_k < 10^{-1}$. Thick gray line: A correction as expected by critical failure $D(E; E_m, E_m f_k^{\beta(\hat{\varepsilon},\hat{m})}, \hat{\varepsilon}(f_k))$ with global $\hat{\varepsilon}$ and estimated $\hat{m}$. The f_k intervals of evaluation grow exponentially and have an imposed minimum size of $n = 100$ signals ($n = 50$ for G26). X-error bars: Integration interval. Y-error bars: 90% bootstrap interval in (d)–(i) and likelihood standard deviation in (d)–(f). Hard lower threshold imposed at $E_m = 1.0$ aJ.

by introducing microscopical mechanisms of transient hardening such as rheology damage [66,67], rate-and-state-dependent friction [68], or viscoelasticity [38,69,70] into models that would otherwise exhibit critical failure [61,62,70]. Transient hardening acts as an effective dissipation [61,62,71] preventing criticality [62,70,72,73] and introduces temporal scales to the model reproducing the foreshock and aftershock sequences [61,69,74]. The latter are perceivable in Fig. 2(a) after P_c^5, for example, and reported in Refs. [4,5] and the Supplemental Material [59].

Some of the last intervals preceding P_c^k exhibit a significant decrease of $\hat{\varepsilon}$ [see Fig. 3(c)] and an increase in $\langle E_{\mathrm{AE}}\rangle$ even higher than the expectation from Eq. (5) and the estimated $\hat{\varepsilon}$. Such intervals might contain superposition of events [75], artifacts due to the signal clipping of large avalanches, or strong AE related to brittle failure. As discussed in Ref. [61], brittle events can follow particular statistical laws. Some experiments of rock fracture report instead a progressive decrease in $\hat{\varepsilon}$ far from failure [1,39,43,76,77], but this is not a universal feature [48], and it is also inconsistent with models [20]. Anisotropic stresses are known to affect ε in structural phase transitions [78], which might or might not play a role in rock fracture [48]. The small size of our samples, close to the width of localization bands in sandstones [48,79], might prevent any band-related anisotropy. Finally, several brittle events might commonly appear under uniaxial compression, since similar results were reported at constant stress [80]. Simulations can reproduce multifragmenation from dynamic fracture [81] or localized weakening bands in a predominantly hardening process [14,20].

Both friction and different fracture mechanisms are involved in mechanical failure under compression [24,82]. We compare the experimental values of ε, γ, and m to the MF solutions of pure fracture and frictional models with transient hardening. We consider the MF stick-slip model [10,60,83,84] as a prototype for frictional avalanches and the democratic fiber bundle model [37] for fracture (see Supplemental Material [59], which includes Refs. [85–87]). The collection of MF exponents [10,61,88] is shown in Table II. The critical exponents [Eqs. (2) and (4)] are defined in terms of the size (S) of the avalanche from the relations

$$D(S;f)dS = S^{-\kappa}\mathcal{D}_S(Sf^{1/\sigma})dS; \qquad \langle S|T\rangle \sim T^{1/\sigma\nu z}. \tag{6}$$

In MF models, the exponents κ, $\sigma\nu z$, ε, and γ are universal and invariant under transient hardening [10,61]. Given the broad regime with $\langle D_{\mathrm{AE}}\rangle \sim E_{\mathrm{AE}}^{1/\gamma}$ (Fig. 1), we assume $E_{\mathrm{AE}} \propto E$. The estimated exponents ε and γ determine the values of κ and $\sigma\nu z$, as shown in Table II. While $\sigma\nu z$ and β are MF, κ and ε are higher but close to MF, below 2 standard deviations in V32 and G26, and 3 standard deviations in SR2, which might indicate the relevance of long-ranged elastic interactions.

TABLE II. Top three rows: Fitted exponents as represented in Figs. 3(g)–3(i), Figs. 2(a)–2(c), and Fig. 3(a)–3(c), compared to the MF exponents for slip and fracture. Bottom six rows: Fundamental exponents estimated from MF theory. The superscripts a [Eq. (7)] and b [Eq. (3)] denote two different interpretations of ASR in terms of MF theory (see text).

	V32	G26	SR2	Slip MF	Fracture MF
γ	3.0 (4)	3.4 (4)	3.2 (4)	3	3
ε	1.40 (5)	1.40 (5)	1.50 (5)	4/3	4/3
m	1.02 (13)	1.11 (20)	0.99 (8)	1^{a} 2^{b}	$1/2^{\mathrm{a}}$ 1^{b}
$\sigma\nu z$	0.50 (6)	0.45 (6)	0.48 (5)	1/2	1/2
κ	1.60 (8)	1.62 (8)	1.76 (8)	3/2	3/2
σ^{a}	0.40 (9)	0.34 (9)	0.24 (8)	1/2	1
σ^{b}	0.88 (12)	0.80 (16)	0.76 (7)	1/2	1
β^{a}	3.7 ± 0.8	4.6 ± 1.2	6.3 ± 2.1	3	3/2
β^{b}	1.67 (24)	1.83 (37)	2.00 (25)	3	3/2

The MF solutions of friction and fracture are similar, but they differ in the values of $1/\sigma$ and β related to the approach to failure (see the Supplemental Material [59]). Furthermore, the interpretation of m in terms of the MF exponents is unclear when transient hardening is present. According to MF models, the exponent m defining the seismic energy released [Eq. (1)] is modified by transient hardening. Following Eq. (6), the mean size in models with critical failure diverges as $\langle S\rangle(f) \sim f^{(\kappa-2)/\sigma}$, and thus $dS/dt \sim f^{(\kappa-2)/\sigma}$. Under slow driving, dS/dt is invariant under transient hardening [61]. Considering the constant $\langle E\rangle(f)$ observed in Figs. 3(d)–3(f), the MF model assumes that $\langle S\rangle(f)$ is also constant. Thus, dS/dt diverges due to the divergence of dN/dt and, instead of Eq. (3), we have

$$dE/dt(f) = \langle E\rangle(f)dN/dt(f) \sim f^{\frac{\kappa-2}{\sigma}}. \tag{7}$$

This interpretation of $dE/dt(f)$ derived from MF theory is presented with superscripts a in Table II. The experimental $m = (2-\kappa)/\sigma \approx 1$ coincides with the MF model of frictional avalanches. However, the values of $1/\sigma \sim 2.5$–4 and $\beta \sim 4$–6 are higher than the MF predictions of both models.

The relation between m and the fundamental exponents is discussed in MF theory, but not in models with local interactions, where transient hardening is known to affect the exponents [69,89]. An alternative hypothesis is that ASR [Eq. (3)] is invariant under transient hardening. Then, $m = (2-\varepsilon)\beta \approx 1$ is compatible with the fracture MF model, and the exponents $\sigma \sim 0.8$ and $\beta \sim 1.8$ are between both models, and notably closer to fracture (superscript b in Table II). The presence of brittle events denoting damage and related to fracture is consistent with this interpretation. Rock fracture experiments at low confining pressure [24] are dominated by tensile fracture (not shear) AE events, a phenomenon related to dilatancy, and also reproduced in numerical simulations [90].

In conclusion, sharp strain drops with massive AE events denoting brittle failure are identified during the compression of nanoporous materials. Instead of critical failure, we find that $\langle E_{\mathrm{AE}} \rangle$ is stationary, and accelerated seismic release (ASR) is exclusively observed in the activity rate (dN_{AE}/dt). Experiments under strain driving reported similar results [48], but failure precedes the divergence time of ASR [t_c in Eq. (1)], especially in materials with low porosity ($\Phi \lesssim 10\%$) [49]. Many theoretical models expect avalanche criticality at failure due to the divergence of correlation lengths [15–17,37,57]. This criticality can be prevented by dissipation [70,72,73], the dynamic weakening or hardening of the material [10,62], or the combined effect [71]. In particular, the ASR and the lack of criticality reported here, together with the temporal correlations reported in Ref. [5], can be reproduced by transient hardening [61]. In our experiment, an effective transient hardening can be caused by one or several internal micromechanical processes such as viscoelasticity [69,91], friction between crack surfaces [74], stress corrosion [92], diffusion of internal fluids [93,94], etc. In contrast, externally measured slip avalanches usually scale to failure and appear unperturbed by transient hardening [25–28]. Analytic solutions of MF models allow us to interpret the experimental results in terms of critical exponents. While the interpretation of the ASR [Eq. (1)] and its associated exponents remains an open question, other exponents are consistent with MF theory. A remaining challenge for the future is to validate this extension of MF models to noncritical failure through new micromechanical experiments able to control the potential mechanisms of transient hardening and dissipation.

J. B. acknowledges the hospitality of the Department of Physics of the UIUC during a visit. We acknowledge fruitful discussion with M. LeBlanc and comments by an anonymous referee. J. B., A. P, and E. V. acknowledge financial support from the Spanish Ministry of Economy (No. MAT2016-75823-R). J. B and J. D. acknowledge financial support from NSERC. K. D. gratefully acknowledges support from the National Science Foundation through Grant No. NSF CBET-1336634, and thanks the KITP for hospitality and Support through Grant No. NSF PHY-1125915.

*jordi.barourbea@ucalgary.ca
†eduard@fmc.ub.edu

[1] K. Mogi, The influence of the dimensions of specimens on the fracture strength of rocks: Comparison between the strength of rock specimens and that of the Earth's crust, Bulletin of the Earthquake Research Institute, University of Tokyo **40**, 175 (1962).
[2] J. Davidsen, S. Stanchits, and G. Dresen, Scaling and Universality in Rock Fracture, Phys. Rev. Lett. **98**, 125502 (2007).
[3] E. K. H. Salje, D. E. Soto-Parra, A. Planes, E. Vives, M. Reinecker, and W. Schranz, Failure mechanism in porous materials under compression: Crackling noise in mesoporous SiO_2, Philos. Mag. Lett. **91**, 554 (2011).
[4] J. Baró, Á. Corral, X. Illa, A. Planes, E. K. H. Salje, W. Schranz, D. E. Soto-Parra, and E. Vives, Statistical Similarity between the Compression of a Porous Material and Earthquakes, Phys. Rev. Lett. **110**, 088702 (2013).
[5] G. F. Nataf, P. O. Castillo-Villa, J. Baró, X. Illa, E. Vives, A. Planes, and E. K. H. Salje, Avalanches in compressed porous SiO_2-based materials, Phys. Rev. E **90**, 022405 (2014).
[6] G. F. Nataf, P. O. Castillo-Villa, P. Sellappan, W. M. Kriven, E. Vives, A. Planes, and E. K. H. Salje, Predicting failure: Acoustic emission of berlinite under compression, J. Phys. Condens. Matter **26**, 275401 (2014).
[7] P. O. Castillo-Villa, J. Baró, A. Planes, E. K. H. Salje, P. Sellappan, W. M. Kriven, and E. Vives, Crackling noise during failure of alumina under compression: The effect of porosity, J. Phys. Condens. Matter **25**, 292202 (2013).
[8] E. K. H. Salje, G. I. Lampronti, D. E. Soto-Parra, J. Baró, A. Planes, and E. Vives, Noise of collapsing minerals: Predictability of the compressional failure in goethite mines, Am. Mineral. **98**, 609 (2013).
[9] J. Baró, A. Planes, E. K. H. Salje, and E. Vives, Fracking and labquakes, Philos. Mag. **96**, 3686 (2016).
[10] K. A. Dahmen, Y. Ben-Zion, and J. T. Uhl, Micromechanical Model for Deformation in Solids with Universal Predictions for Stress-Strain Curves and Slip Avalanches, Phys. Rev. Lett. **102**, 175501 (2009).
[11] K. A. Dahmen, Y. Ben-Zion, and J. T. Uhl, A simple analytic theory for the statistics of avalanches in sheared granular materials, Nat. Phys. **7**, 554 (2011).
[12] R. C. Hidalgo, C. U. Grosse, F. Kun, H. W. Reinhardt, and H. J. Herrmann, Evolution of Percolating Force Chains in Compressed Granular Media, Phys. Rev. Lett. **89**, 205501 (2002).
[13] R. Burridge and L. Knopoff, Model and theoretical seismicity, Bull. Seismol. Soc. Am. **57**, 341 (1967).
[14] K. Duan, C. Y. Kwok, and L. G. Tham, Micromechanical analysis of the failure process of brittle rock, Int. J. Numer. Anal. Methods Geomech. **39**, 618 (2015).
[15] D. Sornette, Mean-field solution of a block-spring model of earthquakes, J. Phys. I (France) **2**, 2089 (1992).
[16] Y. Ben-Zion and J. R. Rice, Earthquake failure sequences along a cellular fault zone in a three-dimensional elastic solid containing asperity and nonasperity regions, J. Geophys. Res. Solid Earth **98**, 14109 (1993).
[17] L. De Arcangelis, S. Redner, and H. J. Herrmann, A random fuse model for breaking processes, J. Phys. (Paris), Lett. **46**, 585 (1985).
[18] S. Zapperi, P. Ray, H. Eugene Stanley, and A. Vespignani, First-Order Transition in the Breakdown of Disordered Media, Phys. Rev. Lett. **78**, 1408 (1997).
[19] Y. Moreno, J. B. Gomez, and A. F. Pacheco, Fracture and Second-Order Phase Transitions, Phys. Rev. Lett. **85**, 2865 (2000).
[20] D. Amitrano, Variability in the power-law distributions of rupture events, Eur. Phys. J. Spec. Top. **205**, 199 (2012).
[21] M. J. Alava, P. K. V. V. Nukala, and S. Zapperi, Statistical models of fracture, Adv. Phys. **55**, 349 (2006).

[22] A. Shekhawat, S. Zapperi, and J. P. Sethna, From Damage Percolation to Crack Nucleation through Finite Size Criticality, Phys. Rev. Lett. **110**, 185505 (2013).

[23] J. Davidsen, G. Kwiatek, E.-M. Charalampidou, T. Goebel, S. Stanchits, M. Rück, and G. Dresen, Triggering Processes in Rock Fracture, Phys. Rev. Lett. **119**, 068501 (2017).

[24] S. Stanchits, S. Vinciguerra, and G. Dresen, Ultrasonic velocities, acoustic emission characteristics and crack damage of basalt and granite, Pure Appl. Geophys. **163**, 975 (2006).

[25] N. Friedman, A. T. Jennings, G. Tsekenis, J.-Y. Kim, M. Tao, J. T. Uhl, J. R. Greer, and K. A. Dahmen, Statistics of Dislocation Slip Avalanches in Nanosized Single Crystals Show Tuned Critical Behavior Predicted by a Simple Mean Field Model, Phys. Rev. Lett. **109**, 095507 (2012).

[26] R. Maaß, M. Wraith, J. T. Uhl, J. R. Greer, and K. A. Dahmen, Slip statistics of dislocation avalanches under different loading modes, Phys. Rev. E **91**, 042403 (2015).

[27] J. Antonaglia, X. Xie, G. Schwarz, M. Wraith, J. Qiao, Y. Zhang, P. K. Liaw, J. T. Uhl, and K. A. Dahmen, Tuned critical avalanche scaling in bulk metallic glasses, Sci. Rep. **4**, 4382 (2014).

[28] D. V. Denisov, K. A. Lörincz, J. T. Uhl, K. A. Dahmen, and P. Schall, Universality of slip avalanches in flowing granular matter, Nat. Commun. **7**, 10641 (2016).

[29] D. V. Denisov, K. A. Lőrincz, W. J. Wright, T. C. Hufnagel, A. Nawano, X. Gu, J. T. Uhl, K. A. Dahmen, and P. Schall, Universal slip dynamics in metallic glasses and granular matter: Linking frictional weakening with inertial effects, Sci. Rep. **7**, 43376 (2017).

[30] J. Rosti, J. Koivisto, and M. J. Alava, Statistics of acoustic emission in paper fracture: Precursors and criticality, J. Stat. Mech. (2010) P02016.

[31] E. K. H. Salje and K. A. Dahmen, Crackling noise in disordered materials, Annu. Rev. Condens. Matter Phys. **5**, 233 (2014).

[32] J. T. Uhl, S. Pathak, D. Schorlemmer, X. Liu, R. Swindeman, B. A. W. Brinkman, M. LeBlanc, G. Tsekenis, N. Friedman, R. Behringer *et al.*, Universal quake statistics: From compressed nanocrystals to earthquakes, Sci. Rep. **5**, 16493 (2015).

[33] W. J. Wright, Y. Liu, X. Gu, K. D. Van Ness, S. L. Robare, X. Liu, J. Antonaglia, M. LeBlanc, J. T. Uhl, T. C. Hufnagel *et al.*, Experimental evidence for both progressive and simultaneous shear during quasistatic compression of a bulk metallic glass, J. Appl. Phys. **119**, 084908 (2016).

[34] C. B. Scruby, An introduction to acoustic emission, J. Phys. E **20**, 946 (1987).

[35] Y. Ben-Zion, Collective behavior of earthquakes and faults: Continuum-discrete transitions, progressive evolutionary changes, and different dynamic regimes, Rev. Geophys. **46**, RG4006 (2008).

[36] D. Sornette and C. G. Sammis, Complex critical exponents from renormalization group theory of earthquakes: Implications for earthquake predictions, J. Phys. I (France) **5**, 607 (1995).

[37] S. Pradhan and B. K. Chakrabarti, Precursors of catastrophe in the Bak-Tang-Wiesenfeld, Manna, and random-fiber-bundle models of failure, Phys. Rev. E **65**, 016113 (2001).

[38] E. Lippiello, W. Marzocchi, L. De Arcangelis, and C. Godano, Spatial organization of foreshocks as a tool to forecast large earthquakes, Sci. Rep. **2**, 846 (2012).

[39] C. H. Scholz, The frequency-magnitude relation of microfracturing in rock and its relation to earthquakes, Bull. Seismol. Soc. Am. **58**, 399 (1968).

[40] I. G. Main, P. G. Meredith, and C. Jones, A reinterpretation of the precursory seismic b-value anomaly from fracture mechanics, Geophys. J. Int. **96**, 131 (1989).

[41] D. Amitrano, Brittle-ductile transition and associated seismicity: Experimental and numerical studies and relationship with the b value, J. Geophys. Res. Solid Earth **108**, 2044 (2003).

[42] T. H. W. Goebel, D. Schorlemmer, T. W. Becker, G. Dresen, and C. G. Sammis, Acoustic emissions document stress changes over many seismic cycles in stick-slip experiments, Geophys. Res. Lett. **40**, 2049 (2013).

[43] X. Jiang, D. Jiang, J. Chen, and E. K. H. Salje, Collapsing minerals: Crackling noise of sandstone and coal, and the predictability of mining accidents, Am. Mineral. **101**, 2751 (2016).

[44] X. Jiang, H. Liu, I. G. Main, and E. K. H. Salje, Predicting mining collapse: Superjerks and the appearance of record-breaking events in coal as collapse precursors, Phys. Rev. E **96**, 023004 (2017).

[45] I. G. Main, A damage mechanics model for power-law creep and earthquake aftershock and foreshock sequences, Geophys. J. Int. **142**, 151 (2000).

[46] X.-c. Yin, H.-z. Yu, V. Kukshenko, Z.-Y. Xu, Z. Wu, M. Li, K. Peng, S. Elizarov, and Q. Li, Load-unload response ratio (LURR), accelerating moment/energy release (AM/ER) and state vector saltation as precursors to failure of rock specimens, in *Computational Earthquake Science, Part II* (Springer, New York, 2004), pp. 2405–2416, DOI: 10.1007/978-3-0348-7875-3_21.

[47] L. Wang, S. Ma, and L. Ma, Accelerating moment release of acoustic emission during rock deformation in the laboratory, Pure Appl. Geophys. **165**, 181 (2008).

[48] S. Lennartz-Sassinek, I. G. Main, M. Zaiser, and C. C. Graham, Acceleration and localization of subcritical crack growth in a natural composite material, Phys. Rev. E **90**, 052401 (2014).

[49] J. Vasseur, F. B. Wadsworth, M. J. Heap, I. G. Main, Y. Lavallée, and D. B. Dingwell, Does an inter-flaw length control the accuracy of rupture forecasting in geological materials? Earth Planet. Sci. Lett. **475**, 181 (2017).

[50] Although ASR was first introduced in seismology [51,52], its validity and applicability for earthquake forecasting are highly questionable [51,53–57].

[51] Y. Ben-Zion and V. Lyakhovsky, Accelerated seismic release and related aspects of seismicity patterns on earthquake faults, in *Earthquake Processes: Physical Modelling, Numerical Simulation and Data Analysis, Part II* (Birkhäuser, Basel, Switzerland, 2002), pp. 2385–2412, DOI: 10.1007/s00024-002-8740-9.

[52] S. C. Jaumé and L. R. Sykes, Evolving towards a critical point: A review of accelerating seismic moment/energy release prior to large and great earthquakes, in *Seismicity Patterns, Their Statistical Significance and Physical Meaning* (Springer,

New York, 1999), pp. 279–305, DOI: 10.1007/978-3-0348-8677-2_5.

[53] J. L. Hardebeck, K. R. Felzer, and A. J. Michael, Improved tests reveal that the accelerating moment release hypothesis is statistically insignificant, J. Geophys. Res. Solid Earth **113**, B08310 (2008).

[54] D. Vere-Jones, R. Robinson, and W. Yang, Remarks on the accelerated moment release model: Problems of model formulation, simulation and estimation, Geophys. J. Int. **144**, 517 (2001).

[55] R. Robinson, S. Zhou, S. Johnston, and D. Vere-Jones, Precursory accelerating seismic moment release (AMr) in a synthetic seismicity catalog: A preliminary study, Geophys. Res. Lett. **32**, L07309 (2005).

[56] E. Hauksson, M. A. Meier, Z. E. Ross, and L. M. Jones, Evolution of seismicity near the southernmost terminus of the San Andreas fault: Implications of recent earthquake clusters for earthquake risk in southern California, Geophys. Res. Lett. **44**, 1293 (2017).

[57] A. Mignan, Retrospective on the accelerating seismic release (ASR) hypothesis: Controversy and new horizons, Tectonophysics **505**, 1 (2011).

[58] L. Girard, J. Weiss, and D. Amitrano, Damage-Cluster Distributions and Size Effect on Strength in Compressive Failure, Phys. Rev. Lett. **108**, 225502 (2012).

[59] See Supplemental Material at http://link.aps.org/supplemental/10.1103/PhysRevLett.120.245501 for theoretical details and complementary results.

[60] K. A. Dahmen, Mean field theory of slip statistics, in *Avalanches in Functional Materials and Geophysics* (Springer, New York, 2017), pp. 19–30, DOI: 10.1007/978-3-319-45612-6_2.

[61] J. Baró and J. Davidsen, Universal avalanche statistics and triggering close to failure in a mean-field model of rheological fracture, Phys. Rev. E **97**, 033002 (2018).

[62] A. P. Mehta, K. A. Dahmen, and Y. Ben-Zion, Universal mean moment rate profiles of earthquake ruptures, Phys. Rev. E **73**, 056104 (2006).

[63] D. E. Grady, The spall strength of condensed matter, J. Mech. Phys. Solids **36**, 353 (1988).

[64] H. Laubie, F. Radjai, R. Pellenq, and F.-J. Ulm, Stress Transmission and Failure in Disordered Porous Media, Phys. Rev. Lett. **119**, 075501 (2017).

[65] J. Baró and E. Vives, Analysis of power-law exponents by maximum-likelihood maps, Phys. Rev. E **85**, 066121 (2012).

[66] V. Lyakhovsky, Y. Ben-Zion, and A. Agnon, A viscoelastic damage rheology and rate- and state-dependent friction, Geophys. J. Int. **161**, 179 (2005).

[67] V. Lyakhovsky, Y. Hamiel, and Y. Ben-Zion, A non-local visco-elastic damage model and dynamic fracturing, J. Mech. Phys. Solids **59**, 1752 (2011).

[68] A. Ruina, Slip instability and state variable friction laws, J. Geophys. Res. Solid Earth **88**, 10359 (1983).

[69] S. Hainzl, G. Zöller, and J. Kurths, Similar power laws for foreshock and aftershock sequences in a spring-block model for earthquakes, J. Geophys. Res. Solid Earth **104**, 7243 (1999).

[70] E. A. Jagla and A. B. Kolton, A mechanism for spatial and temporal earthquake clustering, J. Geophys. Res. Solid Earth **115**, B05312 (2010).

[71] K. Dahmen, D. Ertaś, and Y. Ben-Zion, Gutenberg-Richter and characteristic earthquake behavior in simple mean-field models of heterogeneous faults, Phys. Rev. E **58**, 1494 (1998).

[72] A. Vespignani and S. Zapperi, How self-organized criticality works: A unified mean-field picture, Phys. Rev. E **57**, 6345 (1998).

[73] K. B. Lauritsen, S. Zapperi, and H. Eugene Stanley, Self-organized branching processes: Avalanche models with dissipation, Phys. Rev. E **54**, 2483 (1996).

[74] J. H. Dieterich, Modeling of rock friction: 1. Experimental results and constitutive equations, J. Geophys. Res. Solid Earth **84**, 2161 (1979).

[75] F.-J. Pérez-Reche, B. Tadić, L. Mañosa, A. Planes, and E. Vives, Driving Rate Effects in Avalanche-Mediated First-Order Phase Transitions, Phys. Rev. Lett. **93**, 195701 (2004).

[76] T. Hirata, Omori's power law aftershock sequences of microfracturing in rock fracture experiment, J. Geophys. Res. Solid Earth **92**, 6215 (1987).

[77] D. Lockner, The role of acoustic emission in the study of rock fracture, Int. J. Rock Mech. Min. Sci. Geomech. Abstr. **30**, 883 (1993).

[78] R. Niemann, J. Baró, O. Heczko, L. Schultz, S. Fähler, E. Vives, L. Mañosa, and A. Planes, Tuning avalanche criticality: Acoustic emission during the martensitic transformation of a compressed Ni-Mn-Ga single crystal, Phys. Rev. B **86**, 214101 (2012).

[79] P. Baud, E. Klein, and T.-f. Wong, Compaction localization in porous sandstones: Spatial evolution of damage and acoustic emission activity, J. Struct. Geol. **26**, 603 (2004).

[80] E. K. H. Salje, H. Liu, L. Jin, D. Jiang, Y. Xiao, and X. Jiang, Intermittent flow under constant forcing: Acoustic emission from creep avalanches, Appl. Phys. Lett. **112**, 054101 (2018).

[81] F. Hild, C. Denoual, P. Forquin, and X. Brajer, On the probabilistic-deterministic transition involved in a fragmentation process of brittle materials, Comput. Struct. **81**, 1241 (2003).

[82] J. Fortin, S. Stanchits, G. Dresen, and Y. Guéguen, Acoustic emission and velocities associated with the formation of compaction bands in sandstone, J. Geophys. Res. Solid Earth **111**, B10203 (2006).

[83] D. S. Fisher, K. Dahmen, S. Ramanathan, and Y. Ben-Zion, Statistics of Earthquakes in Simple Models of Heterogeneous Faults, Phys. Rev. Lett. **78**, 4885 (1997).

[84] Y. Ben-Zion, K. A. Dahmen, and J. T. Uhl, A unifying phase diagram for the dynamics of sheared solids and granular materials, Pure Appl. Geophys. **168**, 2221 (2011).

[85] Z. Olami, H. J. S. Feder, and K. Christensen, Self-Organized Criticality in a Continuous, Nonconservative Cellular Automaton Modeling Earthquakes, Phys. Rev. Lett. **68**, 1244 (1992).

[86] F. Kun, F. Raischel, R. C. Hidalgo, and H. J. Herrmann, Extensions of fibre bundle models, in *Modelling Critical and Catastrophic Phenomena in Geoscience* (Springer, New York, 2006), pp. 57–92, DOI: 10.1007/3-540-35375-5_3.

[87] E. Vives, J. Baró, and A. Planes, From labquakes in porous materials to earthquakes, in *Avalanches in Functional Materials and Geophysics* (Springer, New York, 2017), pp. 31–58, DOI: 10.1007/978-3-319-45612-6_3.

[88] M. LeBlanc, A. Nawano, W. J. Wright, X. Gu, J. T. Uhl, and K. A. Dahmen, Avalanche statistics from data with low time resolution, Phys. Rev. E **94**, 052135 (2016).

[89] L. E. Aragón, E. A. Jagla, and A. Rosso, Seismic cycles, size of the largest events, and the avalanche size distribution in a model of seismicity, Phys. Rev. E **85**, 046112 (2012).

[90] F. Camborde, C. Mariotti, and F. V. Donzé, Numerical study of rock and concrete behaviour by discrete element modelling, Computers and Geotechnics **27**, 225 (2000).

[91] F. Mainardi and G. Spada, Creep, relaxation and viscosity properties for basic fractional models in rheology, Eur. Phys. J. Spec. Top. **193**, 133 (2011).

[92] D. Bonamy, S. Prades, C. L. Rountree, L. Ponson, D. Dalmas, E. Bouchaud, K. Ravi-Chandar, and C. Guillot, Nanoscale damage during fracture in silica glass, Int. J. Fract. **140**, 3 (2006).

[93] A. Nur and J. R. Booker, Aftershocks caused by pore fluid flow?, Science **175**, 885 (1972).

[94] W. Ehlers and B. Markert, On the viscoelastic behaviour of fluid-saturated porous materials, Granular Matter **2**, 153 (2000).